



ELSEVIER

Journal of Nuclear Materials 278 (2000) 266–272

Journal of  
nuclear  
materials

www.elsevier.nl/locate/jnucmat

# Hardness and defect structures in EC316LN austenitic alloy irradiated under a simulated spallation neutron source environment using triple ion-beams

E.H. Lee <sup>\*</sup>, J.D. Hunn, N. Hashimoto, L.K. Mansur

*Metals and Ceramics Division, Oak Ridge National Laboratory, P.O. Box 2008, Oak Ridge, TN 37831-6376, USA*

Received 20 May 1999; accepted 17 September 1999

## Abstract

For an assessment of the future US spallation neutron source (SNS) target performance, radiation induced hardening and microstructural evolution were investigated as a function of ion dose for EC316LN stainless steel. Irradiation was carried out using 3.5 MeV Fe<sup>+</sup>, 360 keV He<sup>+</sup>, and 180 keV H<sup>+</sup> simultaneous ion-beams at 200°C to simulate the damage, He and H production in the SNS target vessel wall. At low dose (< 1 dpa), the predominant defects were black dots whose number density saturated rapidly within a few dpa. This was followed by the evolution of interstitial loops whose number density saturated below 15 dpa. Although He-bubbles were not visible, severely scalloped loops suggested that the implanted He/H atoms existed in the form of small clusters. Comparison with reported neutron irradiation data showed that hardening and ductility loss occurred mostly in the black dot regime (< 1 dpa), but that good ductility (>20% elongation) was maintained up to a dose level of  $\approx 10$  dpa. © 2000 Elsevier Science B.V. All rights reserved.

## 1. Introduction

Detailed design and construction of an accelerator-based high power spallation neutron source (SNS) for neutron science applications is underway at Oak Ridge National Laboratory. In this system, a type AISI 316 stainless steel vessel containing a liquid mercury target as the neutron source will be subjected to an intense pulsed proton beam and associated neutron flux, accompanied by heat and stress loads. The requirement for the target vessel is to withstand a pulsed beam of 1 GeV energy protons, which produces 2 MW [1].

Under SNS conditions, the peak damage rate at the vessel nose is expected to be  $\approx 1 \times 10^{-6}$  dpa/s on average and  $\approx 1 \times 10^{-2}$  dpa/s during the microsecond beam pulse period. In addition, gaseous atoms will be produced in the vessel wall by transmutation at a rate of

500–1000 appm H/dpa and 50–200 appm He/dpa. The target vessel will be damaged due to atomic displacements by primary protons, spallation neutrons and recoil atoms, and by the high concentrations of transmutation products such as He and H, and cyclic stresses induced by thermal and pressure pulses. The important radiation effects within the SNS operating temperature range will be hardening and ductility loss. Additional possible sources of damage are fatigue loads, liquid metal embrittlement and temperature gradient mass transfer associated with mercury. These effects are expected to determine the lifetime of the target assembly. A wealth of information on the environment and materials considerations is available in the reports of a series of workshops [2–4]. To appraise the damaging effects on the target, EC316LN SS specimens were irradiated under a simulated SNS irradiation environment by simultaneous irradiation with 3.5 MeV Fe<sup>+</sup>, 360 keV He<sup>+</sup>, and 180 keV H<sup>+</sup> ions. In two previous reports [5,6], the changes in microstructure and hardness by H, He, and Fe ions were systematically investigated by employing single, dual, and triple ion-beam irradiations. In

<sup>\*</sup> Corresponding author. Tel.: +1-423 574 5058; fax: +1-423 574 0641.

*E-mail address:* leech@ornl.gov (E.H. Lee).

this work, radiation induced hardening and microstructural evolution were studied as a function of ion dose for triple ion-beam irradiated EC316LN stainless steel.

## 2. Experimental

The nominal composition of the subject alloy (designated as EC316LN SS by European Community fusion energy materials research group) is, in weight percent, 17.4 Cr, 12.3 Ni, 2.3 Mo, 1.8 Mn, 0.46 Si, 0.02 C, 0.06 N with the balance Fe. Transmission electron microscopy (TEM) disks were annealed at 1050°C for 30 min and electrochemically polished prior to irradiation. Details of the triple ion beam facility can be found in Ref. [7]. The ion energies were chosen to render the maximum damage and gas atom depositions near 800 nm depth, determined by the computer code, Stopping and Range of Ions in Matter (SRIM, 1998 version) [8]. An approximate  $\text{Fe}^+$  current to give a peak damage rate of  $\approx 10^{-3}$  dpa/s was applied continuously with 200 appm He/dpa and 1000 appm H/dpa injection rates. A conversion from ion fluence ( $\text{ions/m}^2$ ) to displacement dose (dpa), calculated using the NRT model [9], is given by

$$\text{dpa} = \frac{0.8}{2E_d} \left( \frac{dE}{dx} \right)_{\text{nuclear}} \frac{\text{ion fluence}}{\text{target atomic density}}, \quad (1)$$

where  $E_d$  is a displacement threshold energy (about 40 eV for steel) and  $(dE/dx)_{\text{nuclear}}$  is the nuclear energy loss per unit length per ion, fraction of ion energy expended to atomic nuclei by ion beam. In SRIM calculation, this is derived by adding phonon and displacement energies together. Most of the damage is caused by the  $\text{Fe}^+$  ions.  $\text{He}^+$  and  $\text{H}^+$  ions contributed only about 1.8% and 0.6% of the damage, respectively. The dose ranges covered for this investigation were from 0.1 to 80 dpa. The operating temperature of the SNS target vessel is expected to be between 80°C and 130°C. Ion irradiations were thus carried out at 200°C in consideration of an upward shift in peak damage temperature with increasing damage rate [10]. With increasing damage rate, the point defect concentration does not rise in proportion with the dose rate because of enhanced recombination of vacancies and interstitials. Consequently, the relative fraction of point defects arriving at sinks (i.e., loops) decreases. To compensate, the point defect flux to sinks can be increased by increasing the temperature.

Hardness changes were measured using a nanoindentation hardness tester, which records hardness (load divided by the contact area of the indenter) as a function of contact indentation depth. It is known that the stress field under the indenter extends to about 7 times the indentation depth [11]. Consequently, for a material

which has only  $\approx 1000$  nm deep irradiated layer, the viscoelastic properties of the underlying substrate are probed increasingly as the indentation depth increases. For this reason, hardness values at 200 nm contact indentation depth were used as reference values to indicate the relative increase in hardness due to the irradiation. The same reference indentation depth was also used in previous work [5,6]. A detailed procedure of hardness measurement and a basis for choosing the reference depth can be found in Refs. [12,13], respectively.

TEM specimens were prepared by electrochemically removing  $\approx 700$  nm from the ion bombarded side and then thinning from the unirradiated side until perforation occurred. This procedure produced TEM foils with thicknesses of  $\approx 100$  nm on average and allowed examination of the microstructure between 700 and 800 nm original depth. For examination, a JEOL FX2000 electron microscope operated at 200 keV was used.

## 3. Results

Hardness values at 200 nm contact indentation depth are plotted as a function of displacement dose in Fig. 1. The scatter in hardness data was attributable to experimental limits in determining dose, indenter tip geometry, surface and subsurface effects imposed upon shallow irradiated depth, and to non-uniform microstructure such as dislocations and hard inclusions. The shaded area in the figure shows the trend of hardness change with dose and also the estimated range of error. The data showed that, upon irradiation to 0.1 dpa, hardness increased rapidly to above 4 GPa from a pristine value of 2.7 GPa but showed only a small increase from 0.1 to 1 dpa and beyond. The hardness saturation at higher doses becomes more apparent if the data is plotted in a

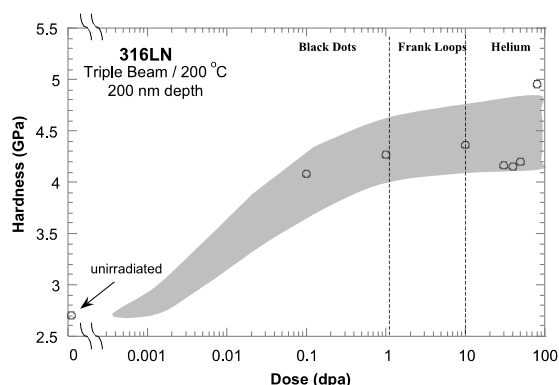


Fig. 1. Hardness variation as a function of ion dose for EC316LN stainless steel irradiated with triple ion-beams at 200°C. The shaded area is the trend of hardness increase with dose and also the range of estimated error.

linear dose scale. More controlled experiments which resolve the scatter are underway. Nonetheless, hardness increase showed a cogent relation to microstructural evolution with dose as described below.

Microstructural examinations were carried out on a different set of TEM disks triple ion-beam irradiated at 200°C to 0.2, 1.7, 15, 30, 36, and 80 dpa. Electron micrographs were taken at zone axis or beam direction  $\mathbf{B}$  near  $\langle 110 \rangle$  and  $\langle 112 \rangle$ , and the corresponding weak-beam dark-field images were taken at  $(g, 3g)$  or  $(g, 5g)$  diffracting condition, or from the diffraction streaks arising from faulted loops. TEM micrographs taken near  $\mathbf{B} \simeq \langle 110 \rangle$  are shown for 1.7, 15, and 80 dpa irradiated specimens in Fig. 2.

At 0.2 dpa, the predominant defects were small defect clusters less than a few nm in diameter which are often called black dots, and few loops were visible at this dose. Although not determined in this work, the damage-induced black dots are believed to be vacancy type stacking-fault tetrahedra (SFT) and small interstitial loops, according to Horiki and Kiritani's investigation [14]. At 1.7 dpa, loops became more visible, while black dot number density approached a saturation value of  $1 \times 10^{23}$ – $2 \times 10^{23} \text{ m}^{-3}$ . Between 1.7 and 15 dpa, interstitial loops evolved continuously but black dot number density remained at about the same level. It should be

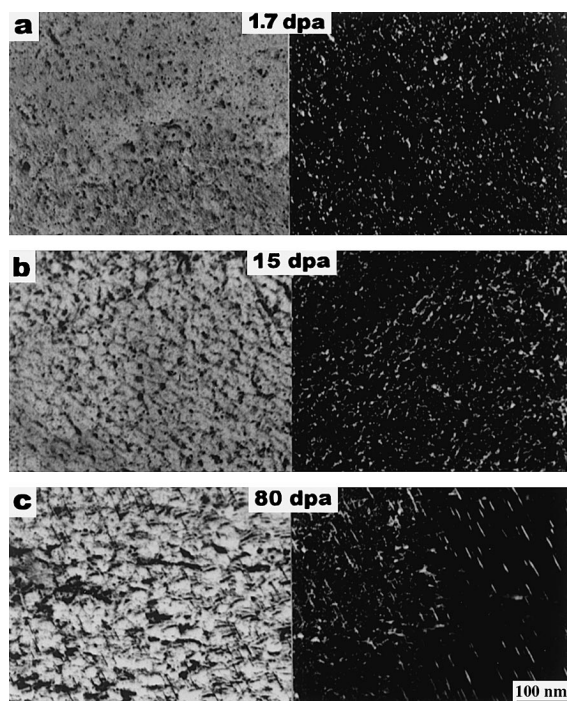


Fig. 2. Bright and dark field TEM micrographs taken near  $\mathbf{B} \simeq \langle 110 \rangle$  for: (a) 1.7 dpa, (b) 15 dpa, and (c) 80 dpa. Black dot number density approached a saturation near or below 1.7 dpa, and Frank interstitial loops evolved between 1 and 15 dpa.

pointed out that most of the hardness increase occurred in the black dot regime.

At 15 dpa, the loop microstructure appeared to be complete resulting in quite an extensive loop network structure. Overall, the defect microstructures of 15 and 80 dpa were very similar as shown in Fig. 3(a) and (b), respectively, in bright and dark-field images taken near  $\mathbf{B} \simeq \langle 112 \rangle$ . It thus appeared that defect microstructure evolution might have reached a saturation near or below 15 dpa. The fishnet-like loop networks shown in the dark-field images of Fig. 3 are due to overlapping loop images in projection. The loops were mostly faulted Frank interstitial loops on  $\{111\}$  planes with a Burger's vector  $\mathbf{b} = a\langle 111 \rangle/3$ . The complex and distorted Moire fringes shown in the bright field images of Fig. 3 are due to overlapping stacking fault fringes arising from the faulted loops on four different  $\{111\}$  planes defined by the Thomson tetrahedron.

The saturation number densities for black dots and Frank loops were  $1 \times 10^{23}$ – $2 \times 10^{23} \text{ m}^{-3}$  and  $22 \times 10^{22}$ – $3 \times 10^{22} \text{ m}^{-3}$ , respectively. Black dots were smaller than a few nm in size and Frank loop sizes were in the range 5–60 nm in diameter at 80 dpa. It should be noted that the Frank loops shown in Fig. 2(c) (dark field) are about one-fourth of the total loops, because there are four  $\{111\}$  planes in fcc. Almost all loops remained faulted with very little indication of unfauling to prismatic loops ( $\mathbf{b} = a\langle 110 \rangle/2$ ) or growth to line dislocations; perhaps the resistance to unfauling may have been due to the low irradiation temperature (200°C) and pinning effect by He/H clusters as described below.

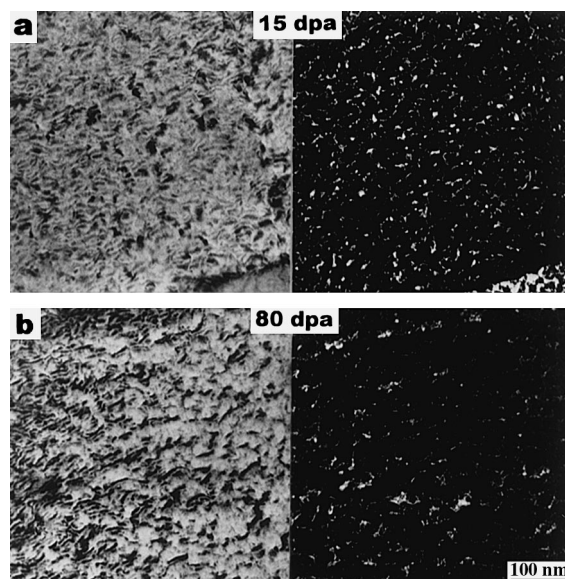


Fig. 3. Bright and dark field TEM micrographs taken near  $\mathbf{B} \simeq \langle 112 \rangle$  for: (a) 15 dpa, and (b) 80 dpa. The loop microstructures of 15 and 80 dpa were similar.

Despite the high concentration of injected helium (1.6 at.% at 80 dpa), no cavities were observed. However, the finely scalloped appearance of the loops indicated that loops are pinned probably by small invisible gas bubbles, (see the dark field loop images in Fig. 3). Helium bubbles are known to exert a pinning effect on loop growth and produce a scalloped loop structure due to bowing between two pivotal bubbles. Such an example was clearly demonstrated for loops formed in Ti-modified stainless steel irradiated at 675°C with 4 MeV Ni and 0.2–0.4 MeV He dual ion-beams [15] and P7 austenitic alloy neutron irradiated in the Oak Ridge Research Reactor (ORR) [16]. Helium clusters are also believed to contain hydrogen based on nuclear reaction analysis data reported previously, in that hydrogen retention was found to be enhanced in the presence of helium [6].

#### 4. Discussion

In the temperature regime of primary interest for SNS components (<200°C), the triple ion-beam irradiation results showed that the defect cluster (black dot) density increased rapidly at a fraction of a dpa and saturated within a few dpa. Thereafter, a conversion of interstitial defect clusters to Frank loops occurred slowly up to  $\leq 15$  dpa. Beyond that, no appreciable change in defect microstructure (black dots and Frank loops) occurred. The microstructure at 80 dpa was very similar to that at 15 dpa, suggesting that the defect microstructure had reached a dynamic steady-state near or below 15 dpa. Since black dots and loops are recombination sites for vacancies and interstitials, the negligible change in defect number density between 15 and 80 dpa is attributable to the high sink density attained at saturation and the ensuing enhanced recombination of point-defects.

The primary microstructural features introduced during triple ion-beam irradiation at 200°C were black dots, Frank loops, and, although not visible, small He/H clusters. From a relationship between number density ( $N$ ) and average distance  $1/(N)^{1/3}$  and our experimentally measured defect number densities at saturation, average distances among black dots and loops were found to be  $\approx 22$  and 32 nm, respectively. Similar microstructural evolution was also observed for austenitic steels irradiated by neutrons and ions [17–19], although microstructural saturation occurred at somewhat varying dose levels near 10 dpa, perhaps due to differences in alloy composition, thermomechanical treatment, irradiation temperature, damage rate, and helium generation rate.

During the triple-beam irradiations, hardness increased rapidly within a few tenths of a dpa and approached a saturation near 1 dpa, following the trend of black dot number density. Only a small increase in

hardening occurred beyond a few dpa, suggesting that vacancy clusters, interstitial loops and helium made small contributions to hardening. A similar trend was also observed for various AISI 316 austenitic steels neutron irradiated below 100°C [20–23]. This temperature is considered to be comparable to the 200°C ion irradiation temperature because of the shift of peak damage temperature for the higher ion damage rate as mentioned already [10]. Figs. 4 and 5 illustrate the dose dependence of yield strength and elongation, respectively, for AISI 316 austenitic steels neutron irradiated below 100°C. The neutron data were compiled from

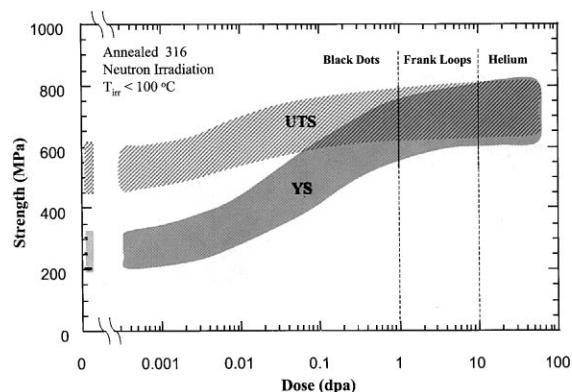


Fig. 4. Yield strength (YS) and ultimate tensile strength (UTS) as a function of dose for AISI 316 stainless steel irradiated by neutrons ( $E > 1$  MeV) below 100°C. Both YS and UTS increase rapidly up to 1 dpa (black dot evolution regime) and thereafter show little change. The original data are from Refs. [19–21].

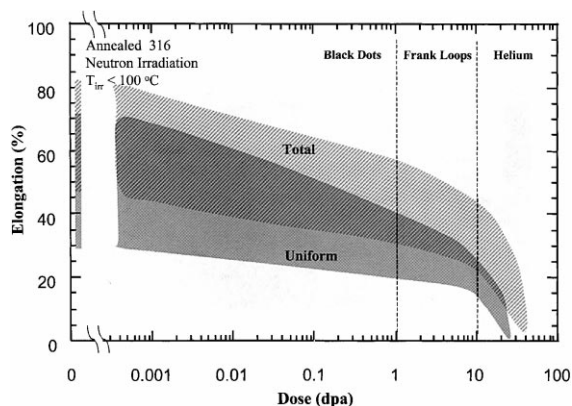


Fig. 5. Uniform and total elongation as a function of dose for AISI 316 stainless steel irradiated by neutrons ( $E > 1$  MeV) below 100°C. The most rapid reduction in elongation occurs below 1 dpa (black dot evolution regime) although it declines continuously with increasing dose. The original data are from Refs. [19–21].

various sources, so there is considerable scatter in data. In spite of the scatter, it is clear that most of the yield strength increase occurred very rapidly within a few tenths of a dpa and showed very small increase beyond 1 dpa, similar to the trend of hardness (Fig. 4). Although the elongation decreased continuously with dose until a complete ductility loss occurred above 10 dpa, again the elongation reduction per unit dose was the highest in the black dot evolution regime ( $< 1$  dpa), see Fig. 5.

It is known that radiation induced defects such as voids, bubbles, precipitates, black dots (vacancy clusters and small loops), Frank loops (large loops), and dislocations inhibit or retard dislocation motion, thereby increasing the flow stress of the material. All of these extended defects are responsible for the changes in mechanical properties for alloys subjected to irradiation [24–29]. Of these barriers, Frank loops are considered to be strong barriers for macroscopic deformation, followed by black dots as intermediate, and gas bubbles as weak barriers [29]. However, since the change in mechanical properties (hardness, yield strength, and elongation) was the largest per unit dose in the black dot dominant regime, the black dot number density seems to be the most important factor in affecting mechanical properties at low temperatures; note that the black dot number density was an order of magnitude higher than that of Frank loops.

Deformation in irradiated steel occurs primarily by normal dislocation slip, twinning, and channeling (annihilation of small defect clusters and loops on slip planes by glissile dislocations) [28–31]. In the channeling process, dislocations clear out defects along the path and subsequent dislocations tend to glide along the cleared path resulting in a channel, free of defects [29]. With increasing dose, dislocation motion, cross slip, and jog formation become progressively more difficult because of increasing interaction with defects (black dots and loops). Moreover, in an fcc system, a moving dislocation interacts with loops oriented in four different  $\{111\}$  planes [32], and the sessile nature of faulted loops, multiplicity of jog formation direction, and pinning by helium clusters all exert augmented barrier effects for moving dislocations. Thus, in a highly defected microstructure, most deformation is likely to occur by channeling with the surrounding defected region remaining undeformed [28]. In irradiated materials, therefore, localized plastic deformation tends to occur on these cleared channels without significant work hardening resulting in a failure with reduced elongation.

Under the SNS condition, the helium generation rate would be 50–200 appm/dpa, over two to three orders of magnitude higher than that of fission neutron irradiation ( $\approx 0.4$  appm/dpa). Loops pinned by He/H clusters are not only difficult to grow but also difficult to shear and thus exert a stronger barrier effect to moving dislocations. This may accentuate localized deformation

induced ductility loss. It is also known that helium accumulation at grain-boundaries causes embrittlement, but probably not at these low temperatures. Thus, a microstructural (black dot and loop) saturation alone may not be a sufficient criterion in evaluating materials; the possible effects of helium/hydrogen must also be considered. In fact, an almost total loss of uniform elongation in tensile tests was observed at a dose level of 3 dpa for austenitic stainless steels irradiated below 100°C by 800 MeV protons at the Los Alamos Neutron Scattering Center (LANSCE) accelerator, where He and H generation rates were comparable to those of SNS [33]. A substantial ductility loss (strain reduction from  $\approx 30\%$  to  $\approx 8\%$ ) was also observed for a AISI 316 L steel implanted with 0.45 at.% helium ( $\approx 0.45$  dpa) at 300°C [34].

A relation between microstructure and macroscopic deformation characteristics is illustrated in Fig. 6. In our triple-beam experiments, microstructural evidence showed that black dot number density was almost an order of magnitude higher than that of loops at the saturation dose. The initial hardening and yield strength increase can be attributed entirely to black dots (Figs. 1 and 4). Although the elongation reduction rate was the largest in the black dot evolution regime (Fig. 5), it declined continuously with dose throughout the entire range of microstructural evolution up to  $\approx 10$  dpa. Since black dots evolved at the earliest dose and in the highest number density, they acted as the major barrier to the onset of plastic deformation ( $< 1$  dpa), whereas Frank loops and He/H clusters produced an additional resistance to plastic deformation at higher doses as they evolved. With increasing temperature, however, the ratio of black dots to Frank loops declines as black dots

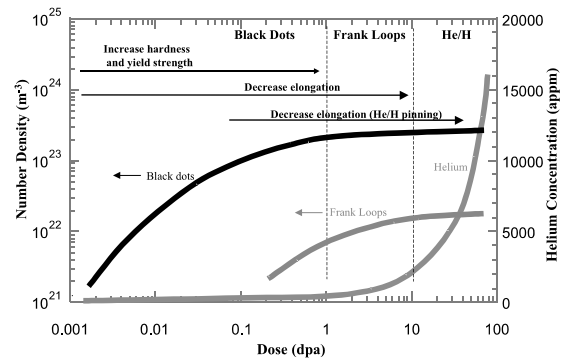


Fig. 6. Schematic representation of microstructural evolution and expected macroscopic mechanical property changes for EC316LN steel irradiated by triple ion-beams at 200°C. This representation may also be relevant for the materials subjected to a fission or fusion reactor irradiation environment, particularly at low temperatures ( $< 400^\circ\text{C}$ ) where dynamic recovery is not significant during irradiation.

convert to loops. With further increase of temperature ( $\geq 350^\circ\text{C}$ ), loops grow faster as the number density declines due to enhanced kinetics, and cavity formation is also facilitated. Thus a maximum loop and cavity barrier strength appeared around 300–330°C for the neutron case [17,20,29].

Although hardness change showed a similar dose dependence as yield strength, neither hardness nor yield stress alone could provide adequate information to evaluate ductility loss by irradiation. They cannot be used as a criterion to determine the degradation of mechanical performance. Importantly, a comparison between neutron data and triple ion-beam microstructure indicated that a severe reduction in uniform elongation (macroscopic deformation) may occur at a dose level where the defect microstructure (black dots and loops) saturates. However, under SNS conditions, ductility loss may occur at a lower dose level because of the high helium and hydrogen generation. This seems to be consistent with the data from a 800 MeV proton irradiation experiment [33].

## 5. Conclusions

For an assessment of the performance of future SNS target materials, hardness change and microstructural evolution during irradiation were investigated for EC316LN austenitic steel irradiated by triple ion beams (3.5 MeV  $\text{Fe}^+$ , 360 keV  $\text{He}^+$ , and 180 keV  $\text{H}^+$ ) at 200°C. The results showed that black dots evolved very rapidly within a few tenths of a dpa and saturated at  $1 \times 10^{23}$ – $2 \times 10^{23} \text{ m}^{-3}$  below  $\approx 2$  dpa. Frank interstitial loops started to evolve below  $\approx 1$  dpa and saturated at  $2 \times 10^{22}$ – $3 \times 10^{22} \text{ m}^{-3}$  near or below 15 dpa. Although cavities were not visible, severely scalloped loop features suggested that loops were decorated by small He/H clusters.

From triple ion-beam, neutron, and 800 MeV proton irradiation data, it was shown that black dots, which appeared at the earliest dose and in the highest number density, dictated the changes in mechanical properties. Thus, most of the increase in hardness and yield strength occurred in the black dot evolution regime ( $< 1$  dpa). Although the highest elongation reduction rate was also in the black dot regime, elongation was reduced continuously as Frank loops and He/H clusters evolved, suggesting that black dots, Frank loops, and He/H clusters, all contributed.

A direct comparison between triple ion-beam and neutron data may not be exact because of the three orders of magnitude difference in damage rate. However, at low temperatures, theoretical calculations based on a kinetic model revealed that the interstitial and vacancy cluster strength would become less sensitive to damage rate because defect supersaturation would dominate

over a thermal annealing effect [27]. Guided by the present ion data, and neutron data obtained previously, a significant ductility loss is expected near a dose level of  $\approx 10$  dpa, at which the loop microstructure saturates and He/H accumulation becomes significant. However, the helium and hydrogen effects should be further studied for a better assessment of the SNS target lifetime.

Finally, an important outcome from this work is the suggestion that macroscopic materials properties might be appraised from small TEM specimens. This mapping would require definitive microstructural correlation to macroscopic deformation behavior as well as a theoretical basis to confirm such a relationship. Information gained from this work is not only of immediate interest for the SNS project, but also provides a stepping stone to establish the fundamental basis to map mechanical properties of radiation-induced microstructure for materials subjected to radiation. Such information would also enable better alloy design for fission and fusion reactor materials.

## Acknowledgements

This research was sponsored by the Division of Materials Sciences, US Department of Energy, under contract No. DE-AC05-96OR22464 with Lockheed Martin Energy Research Corporation. The authors thank Drs K. Farrell and A. F. Rowcliffe for technical review of the manuscript.

## References

- [1] T.A. Gabriel, in: Proceedings of Third International Workshop on Spallation Materials Technology, Santa Fe, New Mexico, 29 April–4 May 1999.
- [2] L.K. Mansur, H. Ullmaier (Eds.), Proceedings of International Workshop on Spallation Materials Technology, Oak Ridge, Tennessee, 23–25 April 1996.
- [3] F. Carsugi, L.K. Mansur, W.F. Sommer, H. Ullmaier (Eds.), Proceedings of Second International Workshop on Spallation Materials Technology, Ancona, Italy, 19–22 September 1997.
- [4] M.S. Wechsler, L.K. Mansur, C.L. Snead, W.F. Sommer (Eds.), Proceedings of the Symposium on Materials for Spallation Neutron Sources, a publication of TMS, Orlando, Florida, 10–12 February 1997.
- [5] E.H. Lee, G.R. Rao, J.D. Hunn, P.M. Rice, M.B. Lewis, S.W. Cook, K. Farrell, L.K. Mansur, in: M.S. Wechsler, L.K. Mansur, C.L. Snead, W.F. Sommer (Eds.), Proceedings of the Symposium on Materials for Spallation Neutron Source, 1997 TMS Annual Meeting, Orlando, Florida, TMS, Warrendale, Pennsylvania, 1998, p. 57.
- [6] J.D. Hunn, M.B. Lewis, E.H. Lee, AccApp98 – Second International Topical meeting on Nuclear Applications of Accelerator Technology, American Nuclear Society, La Grange Park, 1998, p. 375.

- [7] M.B. Lewis, W.R. Allen, R.A. Buhl, N.H. Packan, S.W. Cook, L.K. Mansur, Nucl. Instrum. and Meth. B 43 (1989) 243.
- [8] J.F. Ziegler, J.P. Biersack, U. Littmark, The Stopping and Range of Ions in Solids, Pergamon, NY, 1985.
- [9] M.J. Norgett, M.T. Robinson, I.M. Torrens, Nucl. Eng. Design 33 (1975) 50.
- [10] L.K. Mansur, J. Nucl. Mater. 206 (1993) 306.
- [11] L.E. Samuels, T.O. Mulhearn, J. Mech. Phys. Solids 5 (1957) 125.
- [12] W.C. Oliver, G.M. Pharr, J. Mater. Res. 7 (1992) 1564.
- [13] E.H. Lee, Y. Lee, W.C. Oliver, L.K. Mansur, J. Mater. Res. 8 (1993) 377.
- [14] M. Horiki, M. Kirtani, J. Nucl. Mater. 212–215 (1994) 246.
- [15] E.H. Lee, N.H. Packan, M.B. Lewis, L.K. Mansur, Nucl. Instrum. and Meth. B 16 (1986) 251.
- [16] R.E. Stoller, G.R. Odette, J. Nucl. Mater. 154 (1988) 286.
- [17] S.J. Zinkle, P.J. Maziasz, R.E. Stoller, J. Nucl. Mater. 206 (1993) 266.
- [18] N. Hashimoto, E. Wakai, J.P. Robertson, J. Nucl. Mater. 273 (1999) 95.
- [19] J. Gan, T. Allen, G.S. Was, Mater. Res. Soc. Symp. Proc. 439 (1997) 445.
- [20] J.P. Robertson, I. Ioka, A.F. Rowcliffe, M.L. Grossbeck, S. Jitsukawa, in: R.K. Nanstad, M.L. Hamilton, F.A. Garner, A.S. Kumar (Eds.), Effects of Radiation on Materials: 18th Inter. Symp., ASTM STP 1325, American Society for Testing and Materials, Philadelphia, 1997.
- [21] K. Farrell, L.K. Mansur, in: L.K. Mansur, H. Ullmaier (Eds.), International Workshop on Spallation Materials, 23–25 April 1996, Oak Ridge, TN.
- [22] A.F. Rowcliffe, S.J. Zinkle, J.F. Stubbins, D.J. Edwards, D.J. Alexander, J. Nucl. Mater. 258–263 (1998) 183.
- [23] M.L. Grossbeck, K. Ehrlich, C. Wassilew, J. Nucl. Mater. 174 (1990) 264.
- [24] A.L. Bement Jr., in: Proc. on the Strength of Metals and Alloys, ASM, Metals Park, 1970, p. 693.
- [25] M.L. Grossbeck, P.J. Maziasz, R.F. Rowcliffe, J. Nucl. Mater. 191–194 (1992) 808.
- [26] G.E. Lucas, J. Nucl. Mater. 206 (1993) 287.
- [27] R.E. Stoller, in: A.S. Kumar, D.S. Gelles, R.K. Nanstad, E.A. Little (Eds.), 16th International Symposium ASTM STP 1175, American Society for Testing and Materials, Philadelphia, 1993, p. 394.
- [28] J.I. Cole, S.M. Bruemmer, J. Nucl. Mater. 225 (1995) 53.
- [29] S.M. Bruemmer, J.I. Cole, R.D. Carter, G.S. Was, Mater. Res. Soc. Symp. Proc. 439 (1997) 437.
- [30] F.A. Smidt Jr., Dislocation channeling in irradiated metals, NRL Report 7078, 1971.
- [31] M.S. Wechsler, The Inhomogeneity of Plastic Deformation, American Society For Metals, Metals Park, OH, 1971, p. 19.
- [32] S.G. Song, J.I. Cole, S.M. Bruemmer, Acta Metall. 45 (1997) 501.
- [33] S.A. Maloy, LANL Report TPO-RGN-0013 (1/1999).
- [34] H. Ullmaier, E. Camus, J. Nucl. Mater. 251 (1997) 262.